6936 *Biochemistry* **2010,** *49,* 6936–6944
DOI: 10.1021/bi100358t

BIOCHEMISTRY
including biophysical chemistry & molecular biology
Article

Chemical Basis for the Selectivity of the von Hippel Lindau Tumor Suppressor pVHL for Prolyl-Hydroxylated HIF-1α[†]

Christopher J. R. Illingworth,[‡] Christoph Loenarz,[§] Christopher J. Schofield,[§] and Carmen Domene*,[‡]

[‡]*Department of Chemistry, Physical and Theoretical Chemistry Laboratory, University of Oxford, South Parks Road, Oxford OX1 3QZ, U.K., and* [§]*Chemistry Research Laboratory and Oxford Centre for Integrative Systems Biology, Department of Chemistry, University of Oxford, 12 Mansfield Road, Oxford OX1 3TA, U.K.*

Received March 9, 2010; Revised Manuscript Received June 9, 2010

ABSTRACT: In animals, the post-translational hydroxylation of hypoxia inducible factor (HIF) is a central mechanism for regulating gene expression in an oxygen-dependent manner. The oxygenase-catalyzed *trans*-4-prolyl hydroxylation of HIF-α increases its affinity for the von Hippel Lindau protein elongin B/C (VCB) ubiquitin ligase complex, leading to HIF-α degradation. The level of binding of HIF-α to VCB is increased by ∼1000-fold upon addition of a single oxygen atom to a conserved proline residue. Here, we describe computational studies on the chemical basis of this "switchlike" signaling event. The results support crystallographic analyses showing the importance of hydrogen bonding in the binding of hydroxylated HIF-α to VCB and suggest that *trans* 4-hydroxylation "preorganizes" the proline residue to adopt the C^4-*exo* conformation, via operation of the stereoelectronic gauche effect.

Hypoxia inducible factor (HIF)[1] plays a central role in maintaining oxygen homeostasis in animals, by regulating a large gene array that works to counteract the effects of hypoxia (*1*−*3*). The oxygen sensing component of the HIF system is proposed to involve the post-translational hydroxylation of the HIF-α subunit, as catalyzed by the HIF hydroxylases (*1*, *4*, *5*). In human HIF-1α, hydroxylation of either of two prolyl residues signals the degradation of HIF-α via the ubiquitin proteasome pathway (Figure 1) (*6*−*10*). Asparaginyl hydroxylation in the C-terminal transcriptional activation domain of HIF-α blocks its interaction with p300, thus inhibiting HIF-mediated transcription (*11*). In contrast to the HIF-α subunit, the levels of the HIF-*β* subunit are independent of oxygen availability. When oxygen becomes limiting, HIF-α hydroxylase catalysis slows, causing HIF-α levels to increase; following dimerization with HIF-*β*, and subsequent translocation to the nucleus, the HIF-α/*β* heterodimer binds to hypoxic response elements associated with HIF target genes, enabling their transcription (*3*). At present, the most important of the three human HIF hydroxylases in the hypoxic response is thought to be PHD2 (*12*), which catalyzes prolyl hydroxylation at either of two target sites within both HIF-1α and HIF-2α. The C-terminal of these two oxygen-dependent degradation domains appears to be the preferred target of PHD2, at least under normoxic conditions (*13*).

The discrimination in binding of prolyl-hydroxylated HIF-α, compared to nonhydroxylated HIF-α, to the pVHL−elongin C/B ubiquitin ligase complex (VCB) (*10*, *14*) is a vital component of the proposed sensing mechanism (*15*). *trans*-4-Prolyl hydroxylation of the C-terminal oxygen-dependent degradation domain (CODD) of HIF-1α increases the affinity of HIF-1α peptide fragments for VCB by ∼1000-fold (*16*). Many tumors have been shown to have mutations in pVHL, the targeting subunit of VCB (*17*), supporting the clinical significance of the HIF pathway (*18*). A subset of the clinically observed mutations of pVHL cause weaker binding of HIF-α and are associated with cancer and cardiovascular diseases (*19*).

The remarkable selectivity of the switchlike HIF signaling pathway is proposed to be a key determinant in human oxygen sensing (*1*, *15*, *20*). A recent study has led to the proposal that the conformation of the targeted HIF-α prolyl ring has important roles both in the binding of hydroxylated HIF-α to VCB and in the binding of nonhydroxylated HIF-α to the PHDs (*21*). Crystallographic analyses have revealed that the target proline adopts the C^4-*endo* ring conformation when bound to PHD2 (*22*), but the C^4-*exo* conformation when bound to VCB (Figure 2b) (*16*, *23*). In solution, prolyl residues can adopt either the C^4-*endo* or C^4-*exo* conformation, with a slight preference for the former (*21*, *24*, *25*). Within a *trans*-4-hydroxyprolyl residue, the stereoelectronic effect arising from the $N-C^5-C^4-O$ gauche relationship biases the pyrrolidine ring toward the C^4-*exo* conformation (Figure 2a). The gauche effect arises from the tendency to adopt the conformation with the largest number of gauche interactions between adjacent electron pairs and/or polar bonds (*26*), to maximize delocalization of electron density throughout the *σ*-bond framework (*27*). The gauche effect has

[†]C.D. thanks The Royal Society for a University Research Fellowship. C.L. acknowledges a Rhodes Scholarship. This work was supported by grants from The Leverhulme Trust, the Engineering and Physical Sciences Research Council, the Biotechnology and Biological Sciences Research Council, the Wellcome Trust, and the European Union.

*To whom correspondence should be addressed: Department of Chemistry, Physical and Theoretical Chemistry Laboratory, University of Oxford, South Parks Road, Oxford OX1 3QZ, U.K. Telephone: +44-1865 285401. Fax: +44 1865 275410. E-mail: carmen.domene@chem.ox.ac.uk.

[1]Abbreviations: HIF, hypoxia inducible factor; pVHL, von Hippel Lindau protein; VCB, pVHL elongin B/C ubiquitin ligase complex; PHD2, HIF prolyl hydroxylase domain containing 2; CODD, C-terminal oxygen-dependent degradation domain; MDS, molecular dynamics simulations; HID, N^{δ}-protonated histidine; HIE, N^{ε}-protonated histidine; HIP, both N^{δ}- and N^{ε}-protonated histidine; Hyp-564, Pro-564 hydroxylated; Hyp, hydroxyproline; Flp, fluoroprolyl; PDB, Protein Data Bank; *t*, *trans*; *c*, *cis*.

 Published on Web 07/12/2010

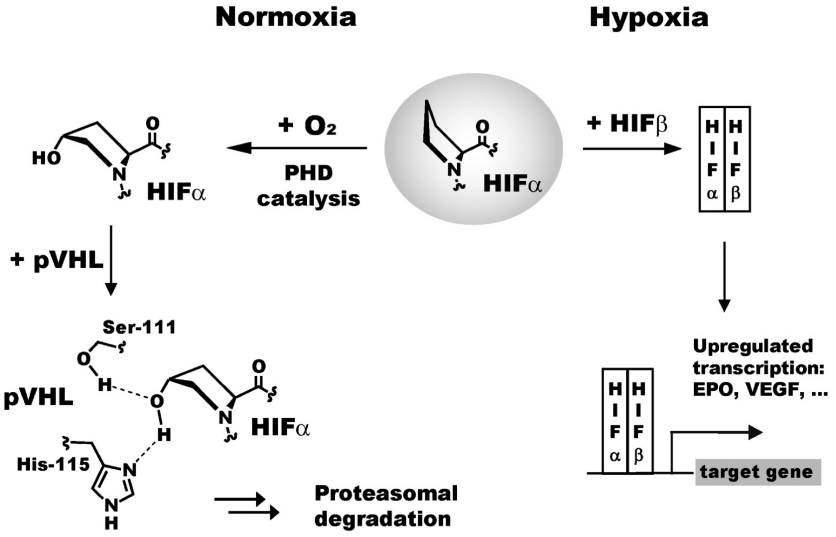

FIGURE 1: Overview of the human HIF oxygen sensing pathway. In normoxia, the PHD enzymes catalyze HIF-α *trans*-4-prolyl hydroxylation, leading to specific recognition of hydroxylated HIF-α by the E3 ubiquitin ligase targeting subunit pVHL, and subsequent proteasomal degradation. Conversely, in hypoxia, the PHD enzymes are less active, leading to accumulation of HIF-α, its translocation to the nucleus, and dimerization with HIF-*β*. The transcriptionally active HIF-α/*β* heterodimer binds to specific recognition motifs on HIF target genes, to activate their transcription.

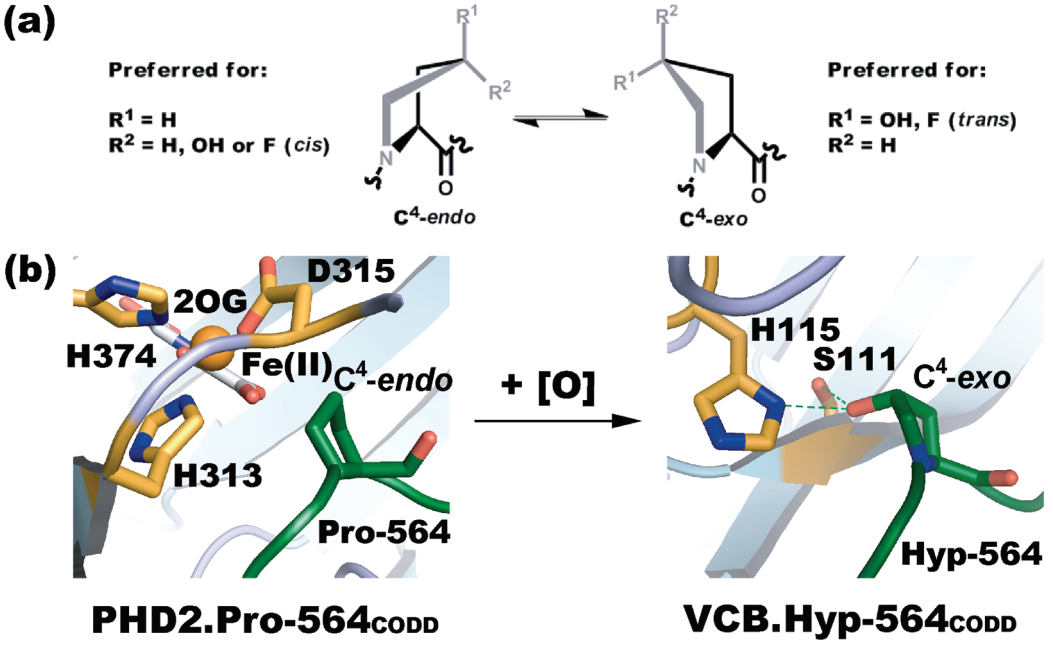

FIGURE 2: HIF-1α Pro-564 residue that adopts a C^4-*endo* conformation when bound to PHD2 and a C^4-*exo* conformation when bound in hydroxylated form to VCB. (a) Electronegative substituents at C-4 bias prolyl residues to prefer either the C^4-*endo* or the C^4-*exo* conformation. (b) Views from the structure of PHD2 and VCB in complex with HIF-1α CODD and Pro-564-hydroxylated CODD, respectively. Note the change in Pro-564_{CODD} conformation from C^4-*endo* to C^4-*exo* upon *trans* 4-hydroxylation. In the PHD2 crystal structure, Fe(II) and 2-oxoglutarate (2OG) were substituted with Mn(II) and *N*-oxalylglycine, respectively, for crystallographic purposes.

been invoked to explain both the conformational preferences of double-helical nucleic acids (*28*) and the stability of the collagen triple helix (*29*). Further work with prolyl-substituted variants of HIF-α has highlighted the importance of hydroxylation in HIF-α recognition by VCB; notably, a variant in which the HIF-α *trans*-4-hydroxyprolyl 564_{CODD} residue is replaced by *trans*-4-fluoroprolyl was not observed to bind to VCB (*21*).

Here we report computational studies aimed at investigating the chemical basis of the selectivity of VCB for hydroxylated HIF-α. We applied molecular dynamics simulations followed by quantum mechanical/molecular mechanical (QM/MM) approaches. Initially, we assessed the ability of a range of computational methods to reproduce the experimentally observed preferences of proline residues for the C^4-*endo* and C^4-*exo* conformations, dependent on different substitutions at C-4. We then employed a QM/MM approach to analyze the binding of HIF-α fragments to VCB, using a residue-by-residue decomposition approach to identify key selectivity-determining interactions. The contribution of stereoelectronic effects to the calculated interaction energy was investigated using an ONIOM method, allowing for electron correlation to be included in a limited region of the system. The results reveal that both hydrogen bonds and

Chart 1: Three Different Forms of the Histidine Side Chain Mentioned Herein[a]

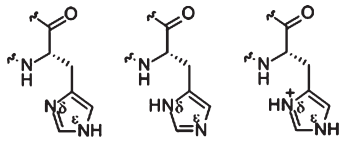

[a] N^{δ}-protonated, HID; N^{ε}-protonated, HIE; both N^{δ}- and N^{ε}-protonated, HIP.

stereoelectronically mediated conformational effects are important in the binding of hydroxylated HIF-α to VCB.

METHODS

Crystal structures of VCB bound to the C-terminal oxygen-dependent degradation domain (CODD) fragment of HIF-α, including hydroxylated P564, have been reported [PDB entries 1LM8 (*23*) and 1LQB (*16*)] at 1.85 and 2.00 Å resolution. We used the higher-resolution structure (PDB entry 1LM8) as a starting model. In all studies, the N-termini of CODD peptides (HIF-$1\alpha_{561-575}$) were acetylated; an *N*-methylamide group was present at the C-termini. Default ionization states were used. Two segments of unresolved residues in the VCB X-ray structures were built using the Wloop homology modeling server (http://bioserv.rpbs.jussieu.fr/cgi-bin/WLoop) (*30*, *31*). These loops correspond to residues 49−58 and 107−118 in elongins C and B, respectively.

Molecular dynamics simulations (MDS) of the VCB-bound CODD peptide were conducted, including all water molecules observed in the crystal structure (PDB entry 1LM8). Additional solvent waters were added using the *Solvate* plug-in of VMD (*32*) using a box padding of 11.5 Å × 11.5 Å × 11.5 Å. Sodium ions were added to neutralize the system. The total system size was ~70600 atoms, including ~64600 water atoms. Five structural models were considered with the following variations in CODD residues and the protonation state of $H115_{VHL}$: (1) *trans*-4-hydroxylated $P564_{CODD}$ and neutral $H115_{VHL}$ protonated at its N^{ε} (HIE form), (2) *trans*-4-hydroxylated $P564_{CODD}$ and neutral $H115_{VHL}$ protonated at its N^{δ} (HID form), (3) $P564_{CODD}$ and $H115_{VHL}$ in the HIE form, (4) $P564_{CODD}$ and $H115_{VHL}$ in the HID form, and (5) *cis*-4-hydroxylated $P564_{CODD}$ and $H115_{VHL}$ in the HIE form (see Chart 1).

For each MDS run, the energy was first minimized by 10000 steps of steepest descent followed by 10 ns of production run. The CHARMM27 force field with CMAP correction (*33*, *34*) was used for VCB, together with the TIP3P model for water molecules (*35*). Default CHARMM parameters were used for ions in bulk solution. The particle mesh Ewald algorithm was used for evaluation of electrostatic interactions (*36*). van der Waals forces were smoothly switched off at 10−12 Å. Bonds with hydrogen atoms were restrained by the SETTLE algorithm (*37*), with a 2 fs time step. The multi-time step algorithm r-RESPA (*38*) was used to integrate the equation of motion. Nonbonded short-range forces were computed for each time step, while electrostatic forces were updated every two time steps. The pressure was kept at 1 atm by the Nose-Hoover Langevin piston (*39*, *40*), with a damping time constant of 100 ps and a period of 200 ps. The temperature was maintained at 300 K by coupling to a Langevin thermostat, with a damping coefficient of 5 ps^{-1}. Calculations were performed using version 2.6 of NAMD (*41*, *42*).

Following from the MDS studies, calculations were conducted on a single "capped" proline residue (N^{α}-acetyl methyl ester) to test the ability of different QM methods to reproduce the experimentally observed conformational preferences with different electronegative substituents at the proline C-4 position (see the Supporting Information). Experimental studies show that electronegative substituents at the *trans*-4 position bias the conformation of the pyrrolidine ring toward the C^4-*exo* conformation, whereas the C^4-*endo* conformation is favored by electronegative substitutions at the *cis*-4 position (Figure 2a) (*24*). Although in previous QM studies on hydroxyprolyl analogues a low-level optimization of the structure has been followed by single-point calculations at higher theoretical levels (*43*, *44*), we performed a full optimization of the molecule at each level of theory. Optimizations were conducted with different substituents at prolyl C-4 in both the C^4-*endo* and C^4-*exo* conformations at a range of levels of theory, both in vacuo and using the IEFPCM implicit solvent model (*45*) as implemented in Gaussian03 (*46*). The difference in calculated energies between the optimized prolyl C^4-*endo* and C^4-*exo* conformations was used as a measure of conformational preference.

QM calculations were then performed on a model of the binding interaction between VCB and HIF-1α CODD peptide variants. The model system was defined from a snapshot of the MDS calculation on *trans*-4-hydroxylated $P564_{CODD}$ and $H115_{VHL}$ in the HIE form, taken after 5 ns of simulation time and considered as representative of the MD configuration ensemble. The CODD peptide was represented by a three-residue fragment consisting of the P564 residue as well as A563 and Y565. The environment of the ligand was represented by including in the model all residues of VCB within 5 Å of $P564_{CODD}$, as measured by closest atom−atom distances. Where necessary, bonds were capped with hydrogen atoms. This resulted in a total of 255 atoms in the QM system, including pVHL residues W88, F91, Y98, I109, H110, S111, Y112, H115, and W117. The system included seven water molecules close to $P564_{CODD}$; none of these waters were present in the crystal structure but instead were part of the explicit aqueous solvent. Examination of the MD trajectory showed individual water molecules moving rapidly in and out of the space close to the $P564_{CODD}$ residue, such that the water molecules as a whole could be considered bulk solvent.

To investigate the effect of proline substitution on the calculated energy for interaction of CODD peptides with VCB, the geometry of the system was optimized, using the B3LYP/6-31G* level of theory (see the Supporting Information for why this level was used). To maintain the relative positions of CODD and the VCB residues, the locations of the backbone atoms of all residues, except for $P564_{CODD}$, were frozen in positions derived from the MDS snapshot. Having obtained an "optimized" structure, we conducted single-point energy calculations to investigate the calculated interaction energy of the three-residue CODD peptide fragment and the central $P564_{CODD}$ residue to VCB: E(calculated interaction between A and B) = E(AB) − E(A) − E(B). To evaluate the behavior of VCB in the case where no CODD peptide was bound, further QM calculations were conducted by replacing the bound peptide with a single water molecule, located according to a crystal structure of VCB without bound CODD peptide, where a water molecule forms a hydrogen bond to $H115_{VHL}$ and $S111_{VHL}$ (*14*).

A residue-by-residue decomposition of the calculated interaction energy was conducted by means of a series of single-point calculations for the interaction of both the three-residue CODD

Table 1: Calculated Interaction Energies of CODD Variants with VCB with Different Protonation States for $H115_{VHL}$[a]

	three-residue fragment interaction energy (kcal/mol)			single-residue fragment interaction energy (kcal/mol)		
	HID	HIE	HIP	HID	HIE	HIP
trans-4-hydroxyprolyl	−80.51	−82.52	−83.99	−29.92	−30.14	−34.52
trans-4-fluoroprolyl	−77.52	−73.94	−81.87	−25.25	−20.60	−31.19
prolyl	−67.93	−66.56	−61.73	−12.54	−10.60	−10.19

[a] N^{δ}-protonated, HID; N^{ε}-protonated, HIE; both N^{δ}- and N^{ε}-protonated, HIP. Three-residue fragment interaction energies detail the calculated interaction energy of the three-residue fragment of CODD to the remainder of the model system. Single-residue fragment interaction energies (with the adjacent CODD residues A563 and Y565 excluded from the calculation) detail the calculated interaction energy of the (non)-substituted $P564_{CODD}$ residue to the remainder of the model system.

fragment and the hydroxylated $P564_{CODD}$ residue with each residue of VCB included in the model. Using this protocol, calculations were performed to establish the likely protonation state of the $H115_{VHL}$ residue, which had not been ascertained in earlier work. The model system was defined as described above, with $H115_{VHL}$ in each of the three possible protonation states [HID, HIE, and HIP (see Chart 1)]. For each protonation state, three systems were studied, with the $P564_{CODD}$ residue modified to prolyl, *trans*-4-hydroxyprolyl, and *trans*-4-fluoroprolyl residues, respectively.

Having established the most likely protonation state of the $H115_{VHL}$ residue as being HIE (see Results), we performed further calculations on systems with the $P564_{CODD}$ residue substituted with *cis*-4-hydroxyprolyl and *cis*-4-fluoroprolyl residues. Calculations were repeated for *trans*-4-hydroxyprolyl, *cis*-4-hydroxyprolyl, and prolyl residues in which the initial conformation of the prolyl ring was changed, prior to optimization, into a C^4-*endo* conformation. Initial structures for the model systems were defined by snapshots taken after 5 ns of MDS. Fluoroprolyl and prolyl $P564_{CODD}$ variants were created by mutation of the snapshot obtained from the VCB−HIF-1α crystal structures with the bound *trans*-4-hydroxyprolyl 564_{CODD} variant (that is, the hydroxyl group was replaced with fluorine or hydrogen and the structure was reoptimized). Following optimization of the models, energy decomposition was performed in each case to measure the contributions of the key binding site residues in the binding of CODD to VCB.

To minimize the effects of random changes in the locations of water molecules carried over from the MDS into the QM system, calculations were repeated for an equivalent system with removal of all water molecules. Energies were recalculated as described above.

To investigate the role of stereoelectronic effects in the binding of CODD to VCB, an ONIOM method was used to incorporate electron correlation into the modeling of the $P564_{CODD}$ residue. The optimized system geometries obtained for the system with the water molecules excluded were reoptimized at the HF/6-31G* level, which excludes electron correlation. A two-layer ONIOM calculation was then performed, with the system as before but with the $P564_{CODD}$ residue modeled at the MP2/6-31G* level, that is, at a level of theory that is identical to HF/6-31G*, but with inclusion of electron correlation (see the Supporting Information). Further calculations were performed in which the side chains of $S111_{VHL}$ and $H115_{VHL}$ were also included at the MP2/6-31G* level.

RESULTS

Initially, we conducted MDS to test the validity of the crystal structures and to investigate the conformational preference of HIF-1α $P564_{CODD}$ and the contribution of $H115_{VHL}$ to HIF-1α−VCB binding. The results of the MDS on the HIF-1α−VCB complex varied in a manner dependent on the protonation state of the $H115_{VHL}$ residue (N^{δ}-protonated, HID; N^{ε}-protonated, HIE; both N^{δ}- and N^{ε}-protonated, HIP). When residue 564_{CODD} was *trans*-4-hydroxyprolyl, with $H115_{VHL}$ in the HIE protonation state, 564_{CODD} exhibited a strict preference for the C^4-*exo* conformation (99:1, *exo*:*endo*). However, when $H115_{VHL}$ was in the HID state, there was a preference for the C^4-*endo* conformation (20:80, *exo*:*endo*). The crystal structures of a HIF-1α peptide fragment bound to VCB show that *trans*-4-hydroxyprolyl 564_{CODD} is in the C^4-*exo* conformation (*16*, *23*). Together, these results imply that for $H115_{VHL}$, the HIE (i.e., the histidine has a neutral charge with a protonated N^{ε}) protonation state is preferred, at least when HIF-α forms a complex with prolyl-hydroxylated CODD. For unsubstituted $P564_{CODD}$, the observed conformational preferences were reversed; when $H115_{VHL}$ was in the HIE state, there was a preference for the C^4-*endo* conformation (22:78, *exo*:*endo*), whereas when $H115_{VHL}$ was in the HID state, the C^4-*exo* conformation was preferred (91:9, *exo*:*endo*). With *cis*-4-hydroxyprolyl at residue 564_{CODD}, and with $H115_{VHL}$ in the HIE state, the C^4-*exo* conformation of residue 564_{CODD} was strictly preferred (99:1 *exo*:*endo*); note that in solution, *cis*-4-hydroxyprolyl substitution is predicted to be biased toward the C^4-*endo* conformation (*24*). Overall, these initial MDS results for prolyl and *trans*-4-hydroxyprolyl 564_{CODD} are consistent with the crystallographic and substrate analogue studies that predict *trans*-4-hydroxyprolyl 564_{CODD} to adopt the C^4-*exo* conformation when bound to VCB (*16*, *21*, *23*).

To further investigate the likely protonation state of the $H115_{VHL}$ residue, optimizations were conducted at the B3LYP/6-31G* level of theory on the model system of the hydroxyprolyl 564_{CODD} binding site of VCB, comprising three HIF-α CODD residues (A563, P564, and Y565) and the surrounding VCB residues, with $H115_{VHL}$ in each of the three possible protonation states (N^{δ}-protonated, N^{ε}-protonated, or both N^{δ}- and N^{ε}-protonated), and with each of three prolyl variants (prolyl, *trans*-4-fluoroprolyl, and *trans*-4-hydroxyprolyl). These calculations resulted in predicted interaction energies for a total of nine systems (Table 1). The fluoroprolyl variants were included because fluorine can act as a hydrogen bond acceptor, but not as a donor.

Experimental work (*16*, *21*) has demonstrated an ~1000-fold selectivity in the binding to VCB of a short HIF-1α *trans*-4-hydroxyprolyl 564_{CODD} peptide as compared to its unmodified $P564_{CODD}$ variant before hydroxylation. With each of the $H115_{VHL}$ protonation states, *trans*-4-hydroxyprolyl 564_{CODD} is predicted to bind considerably stronger than the prolyl 564 variant, with a difference of 15−23 kcal/mol in the calculated

single-residue interaction energies (Table 1). However, the selectivity for a hydroxyprolyl over a fluoroprolyl residue is significantly more pronounced in the HIE than in either the HID or HIP protonation state, matching experimental observations of selectivity (*21*). These results further suggest that $H115_{VHL}$ is likely to occupy the HIE protonation state when bound to *trans*-4-hydroxyprolyl 564_{CODD}.

Optimizations of the same model system were then conducted on other variants of the $P564_{CODD}$ residue with the $H115_{VHL}$ residue in the HIE protonation state at the B3LYP/6-31G* level of theory. Examination of the MD trajectory showed individual waters moving rapidly in and out of the space close to the $P564_{CODD}$ residue. To highlight differences caused by variation in the $P564_{CODD}$ residue, rather than potentially due to the solvent, the solvent waters were omitted from the system before optimization. The same trends in calculated interaction were observed for both the results with the solvent waters omitted (Table 2) and included (Table S3 of the Supporting Information). Although the inclusion or exclusion of the $A563_{CODD}$ and $Y565_{CODD}$ residues from the energy calculation had a substantial impact on the calculated interaction energies obtained (for example, due to the formation of hydrogen bonds between these residues and VCB), exclusion of these residues did not affect the relative trend of the calculated interaction energies of the proline variants.

Of the different $P564_{CODD}$ variants, *trans*-4-hydroxyproline in the C^4-*exo* conformation was observed to have the strongest calculated interaction energy with VCB. The results also imply that the *cis*-4-hydroxyproline residue binds substantially weaker than *trans*-4-hydroxyproline, followed in decreasing order of calculated interaction energy by the fluoroproline variants and finally proline. The ordering of calculated interaction energies in the C-4-substituted $P564_{CODD}$ residues compares favorably with that obtained from experimental binding assays in that, for example, *cis*-4-hydroxyproline binds more strongly than *trans*-4-fluoroproline (*21*).

We note that the ordering of the calculated interaction energies, rather than the absolute values obtained, is most relevant (at least with the current calculations). This is because the calculations performed reproduce changes in the residues involved upon binding in a quantum framework, but do so in a vacuum, and neglect contributions to the energy of binding due to desolvation or changes in entropy. For the results reported in Table 2, the energy cost of removal of water from the binding site of pVHL was assumed to be constant. However, removal of a hydroxyproline residue from solution would incur a larger entropic cost than the removal of a more hydrophobic proline residue, leading to a difference in free energy on binding of the two systems somewhat smaller than the differences reported above. Calculations on a single residue (detailed in the Supporting Information) taking into account desolvation energy suggest a reduction in the difference between the proline and *trans*-4-hydroxyproline residues of ~6 kcal/mol compared to the values reported in Table 2.

To further investigate the differences in calculated interaction energies for the CODD variants, a residue-by-residue interaction energy decomposition was conducted (Table 3; equivalent results for the systems with waters included are reported in Tables S4 and S5 of the Supporting Information). The results reveal that in both the *trans*-4-hydroxyproline and *cis*-4-hydroxyproline variants of $P564_{CODD}$, the hydroxyl group is positioned to form a hydrogen bond with $H115_{VHL}$, leading to an increase in the calculated interaction energy of ~8 kcal/mol relative to the

Table 2: Calculated Interaction Energies for Different Variants of the HIF-1α $P564_{CODD}$ Residue at the B3LYP/6-31G* Level of Theory[a]

	interaction energy (kcal/mol)	
B3LYP/6-31G*	A563-P564-Y565	P564
trans-4-hydroxyprolyl (*exo*)	−50.07	−32.26
trans-4-hydroxyprolyl (*endo*)	−41.10	−25.53
cis-4-hydroxyprolyl (*exo*)	−44.10	−27.42
cis-4-hydroxyprolyl (*endo*)	−31.25	−14.03
trans-4-fluoroprolyl (*exo*)	−40.91	−22.47
cis-4-fluoroprolyl (*exo*)	−35.29	−19.57
prolyl (*exo*)	−29.53	−12.21
prolyl (*endo*)	−27.97	−11.28

[a]The $H115_{VHL}$ residue is in the HIE state in all cases. *exo* and *endo* refer to the prolyl 564_{CODD} conformation at C-4 (see Figure 2a).

Table 3: Residue Decomposition of Single-Residue Interaction Energies Calculated for Different Variants and Conformations of the HIF-1α $P564_{CODD}$ Residue at the B3LYP/6-31G* Level of Theory[a]

	interaction energy (kcal/mol)								
P564 variant	W88	F91	Y98	I109	H110	S111	Y112	H115	W117
t-4-Hyp (*exo*)	0.76	0.03	**−10.48**	0.10	−2.28	**−6.89**	−1.34	**−8.30**	−0.48
t-4-Hyp (*endo*)	−2.40	0.07	**−10.96**	0.04	−1.36	**−4.80**	−0.44	**−0.39**	−3.29
c-4-Hyp (*exo*)	0.66	0.08	**−9.72**	0.00	−3.28	**−4.37**	−1.95	**−9.16**	−0.79
c-4-Hyp (*endo*)	0.37	0.06	**−12.30**	0.00	−2.95	**1.69**	−1.30	**−1.04**	0.53
t-4-Flp (*exo*)	−0.96	0.17	**−10.27**	0.20	−2.80	**−5.72**	−1.59	**0.19**	−0.28
c-4-Flp (*exo*)	−2.18	0.04	**−9.97**	0.07	−1.86	**−3.47**	−0.33	**−0.48**	−1.31
Pro (*exo*)	−0.05	0.03	**−9.97**	0.03	−2.28	**0.13**	−0.25	**−0.99**	0.29
Pro (*endo*)	−0.08	0.02	**−9.85**	0.00	−1.79	**0.58**	−0.24	**−0.73**	0.45
t-4-Hyp HIP (*exo*)	−0.94	0.03	**−10.85**	0.09	−1.65	**−5.02**	−0.5	**−14.97**	−2.81
c-4-Hyp HIP (*exo*)	−0.98	0.05	**−10.47**	0.06	−3.30	**−1.68**	−1.71	**−15.62**	−1.72
t-4-Flp HIP (*exo*)	−0.89	0.07	**−9.18**	0.21	−3.04	**−5.62**	−1.26	**−13.42**	−0.32
Pro HIP (*exo*)	−0.28	−0.04	**−9.77**	0.03	−2.30	**0.07**	−0.19	**1.04**	0.48

[a]Optimizations were conducted with solvent waters removed. Values for VCB residues that make the largest contribution to the difference in calculated interaction between different prolyl 564_{CODD} variants are highlighted in bold (pVHL, Y98, S111, and H115). $H115_{VHL}$ is in the HIE state, unless stated otherwise. To isolate the interactions with the $P564_{CODD}$ residue, only the single-residue binding energies are given. Hence, the total calculated interaction energies reported above may not precisely equal the sum of the residue-calculated interaction energies, because of the neglect of residue−residue interactions in the breakdown of energies.

fluoroproline and proline variants (Figure 2b); note that fluoroproline cannot act as a hydrogen bond donor. A further distinction was observed between the fluoroproline residue and proline, the former capable of receiving a hydrogen bond from the hydroxyl group of $S111_{VHL}$, contributing between 3 and 6 kcal/mol to the calculated interaction of the fluoroproline variants. For each of the *cis*-4-substituted variants, this hydrogen bond with $S111_{VHL}$ was weaker than that observed for the equivalent *trans*-4-substituted variant, favoring interaction of the *trans*-4 variants by 2−3 kcal/mol. The magnitude of these energy differences can be compared with the energy of a hydrogen bond in a vacuum of ~7−8 kcal/mol.

The results imply that the $Y98_{VHL}$ residue, which is positioned to form a hydrogen bond to the backbone carbonyl group of the CODD hydroxyproline residue, makes a significant contribution to the binding of *trans*-4-hydroxyproline 564_{CODD}. This contribution is relatively constant across most variants in HIF-1α residue 564_{CODD}, although it was observed to be weaker for *cis*-4-hydroxyproline, and for *trans*-4-fluoroproline with $H115_{VHL}$ in the HIP state.

Significantly, when HIF-1α residue 564_{CODD} in the complex with VCB was manually changed into a C^4-*endo* conformation and reoptimized in this conformation, *trans*-4-hydroxyproline, *cis*-4-hydroxyproline, and proline each bound weaker than their corresponding C^4-*exo* conformations. These results further support the proposal that VCB is selective for binding the C^4-*exo* hydroxyprolyl conformation, and that this is similar for both *cis* and *trans* substitution at C-4. For *trans*-4-hydroxyproline 564_{CODD}, weaker binding of the C^4-*endo* conformation appears to be largely due to the breaking of the hydrogen bond with $H115_{VHL}$, which in itself contributes a reduction of ~8 kcal/mol. For *cis*-4-hydroxyproline 564_{CODD} (which is not observed to bind in solution), the difference is more pronounced, with neither of the hydrogen bonds predicted to be formed by the hydroxyl group in the C^4-*exo* conformation. In solution, *cis*-4-hydroxyproline 564_{CODD} exists mainly in the C^4-*endo* conformation (*24*), and this is a likely factor in the lack of observed binding of the *cis*-4-hydroxyproline variant to VCB. For the unmodified prolyl residue, the difference between the C^4-*exo* and *endo* conformations is smaller, consistent with an important role for the hydrogen bonds in selectivity. These results are also consistent with those obtained from the MDS, i.e., that *trans*-4-hydroxyproline and *cis*-4-hydroxyproline 564_{CODD} would both preferably occupy the C^4-*exo* rather than the *endo* conformation, when or if bound to VCB.

To model a possible behavior in a low-pH environment, e.g., as observed in some tumors (*47*), a residue-based decomposition of calculated interaction energies was also obtained for $H115_{VHL}$ protonated at both N^{δ} and N^{ε} (see Table 3). A change in the behavior of *trans*-4-hydroxyproline 564_{CODD} (in the C^4-*exo* conformation) was predicted; i.e., the hydroxyl group accepts a hydrogen bond from $H115_{VHL}$ rather than acting as a hydrogen bond donor, as in the neutral case. Importantly, the discrimination between unsubstituted and *trans*-4-hydroxylated $P564_{CODD}$ variants was maintained in the HIP protonation state. Thus, these results predict that selectivity between the prolyl and hydroxyprolyl 564_{CODD} variants will be retained, even at pH < 7, consistent with experimental analyses showing that selectivity for prolyl-hydroxylated CODD occurs at pH ≥ 6 (data not shown).

There is a discrepancy between the calculated interaction results and experimental analyses at the HIP protonation state, in that the *trans*-4-fluoroprolyl 564_{CODD} variant was predicted to bind only ~1.5 kcal/mol weaker than *trans*-4-hydroxyprolyl 564_{CODD} to the $H115_{VHL}$ residue, markedly smaller than the ~8.5 kcal/mol difference observed when $H115_{VHL}$ was in the HIE protonation state. Experimental analyses revealed (*21*) that at both pH 7.5 and 6 (data not shown) the distinction between *trans*-4-hydroxyproline and *trans*-4-fluoroproline variants is maintained. The possibility that this apparent discrepancy reflects an inadequate calculation method or that at lower pH values, protonation at residues away from the HIF-α hydroxyprolyl binding site of VCB may affect binding cannot be ruled out. However, analysis of potential sites of water binding to the hydroxyprolyl binding site on VCB suggests another possible explanation. When $H115_{VHL}$ was in the HIE protonation state, replacement of the CODD peptide with a water molecule gave calculated interaction energies for water similar in magnitude to those obtained for the single residue $P564_{CODD}$ (Table 2). This interaction energy is intermediate between the predicted interaction energies of *trans*-4-fluoroprolyl and *trans*-4-hydroxyprolyl residues with $H115_{VHL}$ in the HIE protonation state (Table 2). The largest contributions to this calculated interaction energy of the water came from hydrogen bonds formed with $S111_{VHL}$ and $H115_{VHL}$. Hence, in the absence of CODD, VCB could bind water in the hydroxyprolyl binding pocket (as observed crystallographically). It may be that this water can be efficiently displaced by *trans*-4-hydroxyprolyl 564_{CODD}, but not so efficiently by the *trans*-4-fluoroprolyl 564_{CODD} variant. Notably, when $H115_{VHL}$ was modified from the HIE to the HIP protonation state, the calculated interaction energy of water increased substantially. An inability to displace this water may account at least in part for the predicted lack of binding of the *trans*-4-fluoroprolyl 564_{CODD} variant at low pH.

The B3LYP/6-31G* method enables calculations for the entire system at a consistent level of theory to be conducted but underestimates the in vacuo preference of *trans*-4-hydroxyproline for the C^4-*exo* conformation; this preference was reproduced only through the use of models that account for electron correlation (Table S7 of the Supporting Information). To investigate the impact of electron correlation on the calculated interaction energies, an ONIOM model was used to isolate the effect of electron correlation in the $P564_{CODD}$ residue. Geometry optimizations of the model system were repeated at the HF/6-31G* level of theory [energies correlated strongly with those calculated using B3LYP (see Table S6 of the Supporting Information)], in which electron correlation is entirely neglected, and then in an ONIOM framework, modeling the $P564_{CODD}$ residue at the MP2/6-31G* level of theory, and the remainder of the system at HF/6-31G*. The MP2 method is identical to HF, but with the addition of electron correlation; thus, comparison of these two models allowed for the isolation of the effect of electron correlation in the proline ring on binding. In addition, use of an ONIOM model allowed for the use of the MP2 level of theory, which was suggested by the single-residue studies to result in an improved model for the conformation of the substituted prolyl residues in solution (the use of this method for the entire protein complex system would be computationally unfeasible) (Table S7 of the Supporting Information). Differences in the total calculated interaction energy with the addition of MP2 electron correlation of up to 2 kcal/mol were observed compared to values without electron correlation. Although the calculated interaction energy was not consistently stronger or weaker for either the prolyl C^4-*exo* or the *endo* conformation, the difference between these

conformations was slightly increased, predicting a stronger preference for the C^4-*exo* conformation in each of the three cases. These increases were small, at 0.82 kcal/mol for the prolyl, 1.50 kcal/mol for the *cis*-4-hydroxyprolyl, and 1.85 kcal/mol for the *trans*-4-hydroxyprolyl $P564_{CODD}$ variants. The results suggest that correlation effects may play a relatively small part in the preference of VCB for binding the C^4-*exo* prolyl 564_{CODD} conformation. Importantly, in all of the model systems, the preference for binding of the C^4-*exo* conformation was retained, matching the results obtained at the B3LYP level.

DISCUSSION

Although there are limitations in the currently available computational methods, overall the results support the proposal that the addition of a single oxygen atom to the HIF-α ODD substantially strengthens its binding to the VCB complex. The calculations, using a range of computational models, also support the general mode of binding of CODD to VCB, as observed in crystallographic analyses (*16*, *23*). Residue decomposition analyses reveal that residues other than the (hydroxylated) $P564_{CODD}$ are important in HIF-α−VCB binding but predict that hydroxylation of $P564_{CODD}$ is sufficient to account for the experimentally observed ~1000-fold difference in binding affinity (equivalent to ~4 kcal/mol) for VCB between hydroxylated and nonhydroxylated CODD. The role of prolyl hydroxylation in the binding of HIF-α to VCB, i.e., that the selectivity of VCB for its HIF-α binding partner is predominantly determined by binding events arising from modifications to residue $P564_{CODD}$ alone, is consistent with the signaling mechanisms for binding to E3 ubiquitin ligases other than VCB, in that post-translational substrate modification rather than interactions with unmodified residues determines their selectivity (*48*).

Both the MDS and ab initio (QM/MM) calculations imply that *trans*-4-hydroxylation of $P564_{CODD}$ enables hydrogen bonds with $H115_{VHL}$ and $S111_{VHL}$. The lack of hydrogen bonding for nonhydroxylated $P564_{CODD}$ with $H115_{VHL}$ and $S111_{VHL}$ rationalizes the pronounced selectivity for hydroxylated HIF-α in binding to VCB. The results predict that optimal binding will occur with $H115_{VHL}$ in its neutral form and with hydrogen at its N^{ε} atom. Notably, however, the results predict that the selectivity for binding of hydroxylated $P564_{CODD}$ will be maintained when $H115_{VHL}$ is in its protonated form. This prediction is consistent with experimental data showing that the selectivity for hydroxylated HIF-α is maintained at pH < 7. Thus, our results imply that a factor other than weakened binding to VCB is responsible for the upregulated levels of HIF-α observed in cancer cells with low pH values under normoxic conditions (*49*−*51*).

Further support for the important role of specific hydrogen bonds in the binding of hydroxylated HIF-1α $P564_{CODD}$ to VCB is provided by analyses of CODD variants containing prolyl analogues, where $P564_{CODD}$ was substituted with a *trans*-4-fluoroprolyl residue (*21*). In this case, when $H115_{VHL}$ is in its neutral state, the lack of binding of the fluorine analogue is rationalized by the absence of a hydrogen bond with $H115_{VHL}$. However, the initial modeling studies suggested that the *trans*-4-fluoroprolyl analogue should bind more strongly at a lower pH (when $H115_{VHL}$ is predicted to be protonated), in contrast to experimental analyses. This discrepancy may be explained by an increased level of competition with water for binding to pVHL H115/S111 at lower pH values, although protonation of other residues may also hinder binding.

Crystallographic and biochemical analyses with $P564_{CODD}$-substituted HIF-1α variants (*21*) have led to the proposal that when bound to PHD2, $P564_{CODD}$ adopts the C^4-*endo* conformation but when bound to VCB, it adopts the C^4-*exo* conformation. Our calculations support the idea of the C^4-*exo* conformation being the preferred conformation of binding for both *trans*- and *cis*-4-hydroxyproline 564_{CODD} to VCB. Use of an ONIOM method predicts that electron correlation effects are likely to play an only relatively small role in the selectivity of VCB for hydroxylated $P564_{CODD}$, as the difference between the overall calculated interaction energies of the C^4-*exo* and -*endo* conformations of *trans*-4-hydroxyproline was only increased by 1−2 kcal/mol with the inclusion of electron correlation effects in the model. Electron correlation effects take into account the stereoelectronic gauche effect, proposed to be responsible for the bias of *trans*-4-hydroxyproline residues toward the C^4-*exo* conformation and of *cis*-4-hydroxyproline to the C^4-*endo* conformation (*21*, *52*). However, the current calculations predict that the importance of electron correlation in directly increasing the stability of the hydroxylated CODD binding to the VCB complex is small, compared to the role of the optimized hydrogen bonds to $S111_{VHL}$ and $H115_{VHL}$ (which rely on the C^4-*exo* conformation).

Although electron correlation appears to have a relatively small effect on the calculated interaction energy for HIF-α−VCB binding, it is more important in determining the ratio of uncomplexed C^4-*endo* and -*exo* conformations of substituted proline residues. When electron correlation effects are omitted, the calculations showed little preference for *trans*-4-hydroxyproline to adopt the C^4-*endo* or C^4-*exo* conformation in vacuo. However, when electron correlation effects are included at the MP2 level, a preference of *trans*-4-hydroxyproline for adopting the C^4-*exo* conformation was found, as observed in solution. Overall, these calculations support proposals arising from previous work that the stereoelectronic gauche effect biases the conformation of substituted proline variants to C^4-*endo* and -*exo* states in a regio- and stereospecific manner (*21*, *24*, *25*). We therefore propose that *trans* 4-hydroxylation of prolyl residues in HIF-α biases the conformation of the targeted prolyl residues to the C^4-*exo* state, i.e., that the stereoelectronic gauche effect preorganizes (*53*) HIF-α for binding to VCB. In the case of the stabilization of the collagen triple helix by *trans*-4-prolyl hydroxylation, it is proposed that such residues preorganize appropriate backbone torsion angles for formation of a triple helix (*27*, *54*). In the case of collagen, multiple hydroxylations contribute to the overall stabilizing effect; this contrasts with the role of prolyl hydroxylation in the HIF system, where *trans*-4-hydroxylation at a single prolyl residue is sufficient to signal for HIF degradation.

ACKNOWLEDGMENT

We thank the Oxford Supercomputing Centre for providing computational support.

SUPPORTING INFORMATION AVAILABLE

Details of calculations on the conformational preference of proline variants in implicit solvent (Table S1), calculated interaction energies of CODD with waters included in the optimization (Table S2), version of Table 3 including the calculated interaction energies of the residues adjacent to Hyp-564, with waters added to the system (Table S3), version of Table 3 detailing the calculated interaction energies of Hyp-564, with

waters added to the system (Table S4), details of repeat calculated interaction energy calculations at the HF/6-31G* level (Table S5), calculated interaction energies for the three-residue CODD fragment, and for the single residue $P564_{CODD}$, calculated for structures reoptimized at the HF/6-31G* level of theory (Table S6), and calculated interaction energies for different variants of HIF-α hydroxyprolyl with electron correlation effects in the prolyl ring either included or excluded from the model (Table S7). This material is available free of charge via the Internet at http://pubs.acs.org.

REFERENCES

1. Schofield, C. J., and Ratcliffe, P. J. (2004) Oxygen sensing by HIF hydroxylases. *Nat. Rev. Mol. Cell Biol. 5*, 343–354.
2. Semenza, G. L. (2001) HIF-1 and mechanisms of hypoxia sensing. *Curr. Opin. Cell Biol. 13*, 167–171.
3. Maxwell, P. H., Pugh, C. W., and Ratcliffe, P. J. (2001) The pVHL-HIF-1 system. A key mediator of oxygen homeostasis. *Adv. Exp. Med. Biol. 502*, 365–376.
4. Loenarz, C., and Schofield, C. J. (2008) Expanding chemical biology of 2-oxoglutarate oxygenases. *Nat. Chem. Biol. 4*, 152–156.
5. Kaelin, W. G., Jr., and Ratcliffe, P. J. (2008) Oxygen sensing by metazoans: The central role of the HIF hydroxylase pathway. *Mol. Cell 30*, 393–402.
6. Epstein, A. C. R., Gleadle, J. M., McNeill, L. A., Hewitson, K. S., O'Rourke, J., Mole, D. R., Mukherji, M., Metzen, E., Wilson, M. I., Dhanda, A., Tian, Y.-M., Masson, N., Hamilton, D. L., Jaakkola, P., Barstead, R., Hodgkin, J., Maxwell, P. H., Pugh, C. W., Schofield, C. J., and Ratcliffe, P. J. (2001) *C. elegans* EGL-9 and mammalian homologs define a family of dioxygenases that regulate HIF by prolyl hydroxylation. *Cell 107*, 43–54.
7. Bruick, R. K., and McKnight, S. L. (2001) A conserved family of prolyl-4-hydroxylases that modify HIF. *Science 294*, 1337–1340.
8. Jaakkola, P., Mole, D. R., Tian, Y.-M., Wilson, M. I., Gielbert, J., Gaskell, S. J., Kriegsheim, A. v., Hebestreit, H. F., Mukherji, M., Schofield, C. J., Maxwell, P. H., Pugh, C. W., and Ratcliffe, P. J. (2001) Targeting of HIF-α to the von Hippel-Lindau ubiquitylation complex by O_2-regulated prolyl hydroxylation. *Science 292*, 468–472.
9. Ivan, M., Kondo, K., Yang, H., Kim, W., Valiando, J., Ohh, M., Salic, A., Asara, J. M., Lane, W. S., and Kaelin, W. G., Jr. (2001) HIFα targeted for VHL-mediated destruction by proline hydroxylation: Implications for O_2 sensing. *Science 292*, 464–468.
10. Maxwell, P. H., Wiesener, M. S., Chang, G.-W., Clifford, S. C., Vaux, E. C., Cockman, M. E., Wykoff, C. C., Pugh, C. W., Maher, E. R., and Ratcliffe, P. J. (1999) The tumour suppressor protein VHL targets hypoxia-inducible factors for oxygen-dependent proteolysis. *Nature 399*, 271–275.
11. Lando, D., Peet, D. J., Whelan, D. A., Gorman, J. J., and Whitelaw, M. L. (2002) Asparagine hydroxylation of the HIF transactivation domain: a hypoxic switch. *Science 295*, 858–861.
12. Berra, E., Benizri, E., Ginouves, A., Volmat, V., Roux, D., and Pouyssegur, J. (2003) HIF prolyl-hydroxylase 2 is the key oxygen sensor setting low steady-state levels of HIF-1α in normoxia. *EMBO J. 22*, 4082–4090.
13. Chan, D. A., Sutphin, P. D., Yen, S.-E., and Giaccia, A. J. (2005) Coordinate regulation of the oxygen-dependent degradation domains of hypoxia-inducible factor 1α. *Mol. Cell. Biol. 25*, 6415–6426.
14. Stebbins, C. E., Kaelin, W. G., Jr., and Pavletich, N. P. (1999) Structure of the VHL-ElonginC-ElonginB complex: implications for VHL tumor suppressor function. *Science 284*, 455–461.
15. Kaelin, W. G., Jr. (2005) The von Hippel-Lindau protein, HIF hydroxylation, and oxygen sensing. *Biochem. Biophys. Res. Commun. 338*, 627–638.
16. Hon, W. C., Wilson, M. I., Harlos, K., Claridge, T. D. W., Schofield, C. J., Pugh, C. W., Maxwell, P. H., Ratcliffe, P. J., Stuart, D. I., and Jones, E. Y. (2002) Structural basis for the recognition of hydroxyproline in HIF-1α by pVHL. *Nature 417*, 975–978.
17. Lonser, R. R., Glenn, G. M., Walther, M., Chew, E. Y., Libutti, S. K., Linehan, W. M., and Oldfield, E. H. (2003) von Hippel-Lindau disease. *Lancet 361*, 2059–2067.
18. Ivan, M., and Kaelin, W. G. (2001) The von Hippel-Lindau tumor suppressor protein. *Curr. Opin. Genet. Dev. 11*, 27–34.
19. Clifford, S. C., Cockman, M. E., Smallwood, A. C., Mole, D. R., Woodward, E. R., Maxwell, P. H., Ratcliffe, P. J., and Maher, E. R. (2001) Contrasting effects on HIF-1α regulation by disease-causing pVHL mutations correlate with patterns of tumourigenesis in von Hippel-Lindau disease. *Hum. Mol. Genet. 10*, 1029–1038.
20. Semenza, G. L. (2004) Hydroxylation of HIF-1: Oxygen sensing at the molecular level. *Physiology 19*, 176–182.
21. Loenarz, C., Mecinovic, J., Chowdhury, R., McNeill, L. A., Flashman, E., and Schofield, C. J. (2009) Evidence for a stereoelectronic effect in human oxygen sensing. *Angew. Chem., Int. Ed. 48*, 1784–1787.
22. Chowdhury, R., McDonough, M. A., Mecinovi, J., Loenarz, C., Flashman, E., Hewitson, K. S., Domene, C., and Schofield, C. J. (2009) Structural basis for binding of hypoxia-inducible factor to the oxygen-sensing prolyl hydroxylases. *Structure 17*, 981–989.
23. Min, J.-H., Yang, H., Ivan, M., Gertler, F., Kaelin, W. G., Jr., and Pavletich, N. P. (2002) Structure of an HIF-1α-pVHL complex: Hydroxyproline recognition in signaling. *Science 296*, 1886–1889.
24. DeRider, M. L., Wilkens, S. J., Waddell, M. J., Bretscher, L. E., Weinhold, F., Raines, R. T., and Markley, J. L. (2002) Collagen stability: Insights from NMR spectroscopic and hybrid density functional computational investigations of the effect of electronegative substituents on prolyl ring conformations. *J. Am. Chem. Soc. 124*, 2497–2505.
25. Taylor, C. M., Hardre, R., and Edwards, P. J. B. (2005) The impact of pyrrolidine hydroxylation on the conformation of proline-containing peptides. *J. Org. Chem. 70*, 1306–1315.
26. Wolfe, S. (1972) Gauche effect: Some stereochemical consequences of adjancent electron pairs and polar bonds. *Acc. Chem. Res. 5*, 102.
27. Hodges, J. A., and Raines, R. T. (2005) Stereoelectronic and steric effects in the collagen triple helix: Toward a code for strand association. *J. Am. Chem. Soc. 127*, 15923–15932.
28. Guschlbauer, W., and Jankowski, K. (1980) Nucleoside conformation is determined by the electronegativity of the sugar substituent. *Nucleic Acids Res. 8*, 1421–1433.
29. Eberhardt, E. S., Panasik, N., and Raines, R. T. (1996) Inductive effects on the energetics of prolyl peptide bond isomerisation: Implications for collagen folding and stability. *J. Am. Chem. Soc. 118*, 12261–12266.
30. Kwasigroch, J. M., Chomilier, J., and Mornon, J. P. (1996) A global taxonomy of loops in globular proteins. *J. Mol. Biol. 259*, 855–872.
31. Wojcik, J., Mornon, J. P., and Chomilier, J. (1999) New efficient statistical sequence-dependent structure prediction of short to medium-sized protein loops based on an exhaustive loop classification. *J. Mol. Biol. 289*, 1469–1490.
32. Humphrey, W., Dalke, A., and Schulten, K. (1996) VMD: Visual molecular dynamics. *J. Mol. Graphics 14*, 33.
33. MacKerell, A. D., Bashford, D., Bellott, M., Dunbrack, R. L., Evanseck, J. D., Field, M. J., Fischer, S., Gao, J., Guo, H., Ha, S., Joseph-McCarthy, D., Kuchnir, L., Kuczera, K., Lau, F. T. K., Mattos, C., Michnick, S., Ngo, T., Nguyen, D. T., Prodhom, B., Reiher, W. E., Roux, B., Schlenkrich, M., Smith, J. C., Stote, R., Straub, J., Watanabe, M., Wiorkiewicz-Kuczera, J., Yin, D., and Karplus, M. (1998) All-atom empirical potential for molecular modeling and dynamics studies of proteins. *J. Phys. Chem. B 102*, 3586–3616.
34. Brooks, B. R., Bruccoleri, R. E., Olafson, B. D., States, D. J., Swaminathan, S., and Karplus, M. (1983) CHARMM: A program for macromolecular energy, minimisation, and dynamics calculations. *J. Comput. Chem. 4*, 187–217.
35. Jorgensen, W. L., Chandrasekhar, J., Madura, J. D., Impey, R. W., and Klein, M. L. (1983) Comparison of simple potential functions for simulations of liquid water. *J. Chem. Phys. 79*, 926–935.
36. Essmann, U., Perera, L., Berkowitz, M. L., Darden, T., Lee, H., and Pedersen, L. G. (1995) A smooth particle mesh Ewald method. *J. Chem. Phys. 103*, 8577–8593.
37. Miyamoto, S., and Kollman, P. A. (1992) SETTLE: An analytical version of the Shake and Rattle algorithm for rigid water models. *J. Comput. Chem. 13*, 952–962.
38. Tuckerman, M., Berne, B. J., and Martyna, G. J. (1992) Reversible multiple time scale molecular-dynamics. *J. Chem. Phys. 97*, 1990–2001.
39. Martyna, G. J., Tobias, D. J., and Klein, M. L. (1994) Constant pressure molecular-dynamics algorithms. *J. Chem. Phys. 101*, 4177–4189.
40. Feller, S. E., Zhang, Y. H., Pastor, R. W., and Brooks, B. R. (1995) Constant-pressure molecular dynamics simulation: The Langevin piston method. *J. Chem. Phys. 103*, 4613–4621.
41. Phillips, J. C., Braun, R., Wang, W., Gumbart, J., Tajkhorshid, E., Villa, E., Chipot, C., Skeel, R. D., Kale, L., and Schulten, K. (2005) Scalable molecular dynamics with NAMD. *J. Comput. Chem. 26*, 1781–1802.
42. Kale, L., Skeel, R., Bhandarkar, M., Brunner, R., Gursoy, A., Krawetz, N., Philips, J., Shinozaki, A., Varadarajan, K., and Schuten, K. (1999)

Molecular dynamics programs design-NAMD2: greater scalability for parallel molecular dynamics. *J. Comput. Phys. 151*, 283–312.
43. Improta, R., Mele, F., Crescenzi, O., Benzi, C., and Barone, V. (2002) Understanding the role of stereoelectronic effects in determining collagen stability. 2. A quantum mechanical/molecular mechanical study of (proline-proline-glycine)$_n$ polypeptides. *J. Am. Chem. Soc. 124*, 7857–7865.
44. Improta, R., Benzi, C., and Barone, V. (2001) Understanding the role of stereoelectronic effects in determining collagen stability. 1. A quantum mechanical study of proline, hydroxyproline, and fluoroproline dipeptide analogues in aqueous solution. *J. Am. Chem. Soc. 123*, 12568–12577.
45. Cances, E., Mennucci, B., and Tomasi, J. (1997) A new integral equation formalism for the polarizable continuum model: Theoretical background and applications to isotropic and anisotropic dielectrics. *J. Chem. Phys. 107*, 3032–3041.
46. Frisch, M. J., Trucks, G. W., Schlegel, H. B., Scuseria, G. E., Robb, M. A., Cheeseman, J. R., Montgomery, J. A., Jr., Vreven, T., Kudin, K. N., Burant, J. C., Millam, J. M., Iyengar, S. S., Tomasi, J., Barone, V., Mennucci, B., Cossi, M., Scalmani, G., Rega, N., Petersson, G. A., Nakatsuji, H., Hada, M., Ehara, M., Toyota, K., Fukuda, R., Hasegawa, J., Ishida, M., Nakajima, T., Honda, Y., Kitao, O., Nakai, H., Klene, M., Li, X., Knox, J. E., Hratchian, H. P., Cross, J. B., Bakken, V., Adamo, C., Jaramillo, J., Gomperts, R., Stratmann, R. E., Yazyev, O., Austin, A. J., Cammi, R., Pomelli, C., Ochterski, J. W., Ayala, P. Y., Morokuma, K., Voth, G. A., Salvador, P., Dannenberg, J. J., Zakrzewski, V. G., Dapprich, S., Daniels, A. D., Strain, M. C., Farkas, O., Malick, D. K., Rabuck, A. D., Raghavachari, K., Foresman, J. B., Ortiz, J. V., Cui, Q., Baboul, A. G., Clifford, S., Cioslowski, J., Stefanov, B. B., Liu, G., Liashenko, A., Piskorz, P., Komaromi, I., Martin, R. L., Fox, D. J., Keith, T.; Al-Laham, M. A., Peng, C. Y., Nanayakkara, A., Challacombe, M., Gill, P. M. W., Johnson, B., Chen, W., Wong, M. W., Gonzalez, C., and Pople, J. A. (2004) Gaussian 03, revision C.02, Gaussian, Inc., Wallingford, CT.
47. Lunt, S., Chaudary, N., and Hill, R. (2009) The tumor microenvironment and metastatic disease. *Clin. Exp. Metastasis 26*, 19–34.
48. Ciechanover, A., Orian, A., and Schwartz, A. L. (2000) The ubiquitin-mediated proteolytic pathway: Mode of action and clinical implications. *J. Cell. Biochem. 34*, 40–51.
49. Sudarshan, S., Sourbier, C., Kong, H.-S., Block, K., Romero, V. A. V., Yang, Y., Galindo, C., Mollapour, M., Scroggins, B., Goode, N., Lee, M.-J., Gourlay, C. W., Trepel, J., Linehan, W. M., and Neckers, L. (2009) Fumarate hydratase deficiency in renal cancer induces glycolytic addiction and hypoxia-inducible transcription factor 1α stabilization by glucose-dependent generation of reactive oxygen species. *Mol. Cell. Biol. 29*, 4080–4090.
50. Knowles, H. J., Mole, D. R., Ratcliffe, P. J., and Harris, A. L. (2006) Normoxic stabilization of hypoxia-inducible factor-1α by modulation of the labile iron pool in differentiating U937 macrophages: Effect of natural resistance-associated macrophage protein 1. *Cancer Res. 66*, 2600–2607.
51. Chan, D. A., Sutphin, P. D., Denko, N. C., and Giaccia, A. J. (2002) Role of prolyl hydroxylation in oncogenically stabilized hypoxia-inducible factor-1a. *J. Biol. Chem. 277*, 40112–40117.
52. Fujimori, D. G. (2009) Hypoxia sensing goes gauche. *Nat. Chem. Biol. 5*, 202–203.
53. Warshel, A. (1998) Electrostatic origin of the catalytic power of enzymes and the role of preorganized active sites. *J. Biol. Chem. 273*, 27035–27038.
54. Shoulders, M. D., Kamer, K. J., and Raines, R. T. (2009) Origin of the stability conferred upon collagen by fluorination. *Bioorg. Med. Chem. Lett. 19*, 3859–3862.